BIOCHEMISTRY
including biophysical chemistry & molecular biology
Article

Biochemistry **2009,** *48,* 11211–11219 11211
DOI: 10.1021/bi9015154

Nuclear Magnetic Resonance Structural Characterization of Substrates Bound to the α-2,6-Sialyltransferase, ST6Gal-I[†]

Shan Liu, Lu Meng, Kelley W. Moremen, and James H. Prestegard*

Complex Carbohydrate Research Center, University of Georgia, Athens, Georgia 30602

Received August 28, 2009; Revised Manuscript Received October 21, 2009

ABSTRACT: The α-2,6-sialyltransferase (ST6Gal-I) is a key enzyme that regulates the distribution of sialic acid-containing molecules on mammalian cell surfaces. However, the fact that its native form is membrane-bound and glycosylated has made structural characterization by X-ray crystallography of this eukaryotic protein difficult. Its large size (~40 kDa for just the catalytic domain) also poses a challenge for complete structure determination by nuclear magnetic resonance (NMR). However, even without complete structure determination, there are NMR strategies that can return targeted information about select regions of the protein, including information about the active site as seen from the perspective of its bound ligands. Here, in a continuation of a previous study, a spin-labeled mimic of a glycan acceptor ligand is used to identify additional amino acids located in the protein active site. In addition, the spin-labeled donor is used to characterize the relative placement of the two bound ligands. The ligand conformation and protein−ligand contact surfaces are studied by transferred nuclear Overhauser effects (trNOEs) and saturation transfer difference (STD) experiments. The data afforded by the methods mentioned above lead to a geometric model of the bound substrates that in many ways carries an imprint of the ST6Gal-I binding site.

Nuclear magnetic resonance (NMR)[1] methods, focused on bound ligand properties rather than complete protein structures, can provide a very detailed view of some of the most critical regions of protein systems, including the active sites of enzymes (*1*−*4*). Previously, in one type of NMR experiment, we reported using a spin-labeled donor analogue of a sugar nucleotide, CMP-4-*O*-(4-carboxy-2,2,6,6-tetramethylpiperidine-1-oxyl) (CMP-4carboxyTEMPO), to map the positions of isotopically labeled phenylalanines relative to the position of the analogue in the active site of the α-2,6-sialyltransferase (ST6Gal-I) (*5*). The paramagnetic TEMPO derivative perturbs NMR resonances of the protein in a manner dependent on the inverse sixth power of the distances between the unpaired electron of the nitroxide moiety in TEMPO and the nuclei giving rise to the NMR resonances. Sixteen NMR cross-peaks were observable in $^{1}H-^{15}N$ HSQC spectra when the protein was expressed in HEK 293 cells grown on media containing ^{15}N-labeled phenylalanine; the sites were ranked in the order of their distance to the bound donor mimic based on the perturbation of cross-peak intensity. Glycosyltransferases, however, have two ligands, a donor and an acceptor, offering the opportunity to use similar ligand-based NMR methods to map a more extended binding site (*1*, *6*). Here previous studies are first extended using a spin-labeled acceptor analogue to map distances to additional labeled amino acid sites. Then related paramagnetic strategies are used to characterize the position of the sugar acceptor relative to the donor analogue while both are simultaneously bound to ST6Gal-I. When combined with more traditional transferred NOE (trNOE) (*7*) and saturation transfer difference (STD) (*8*) methodology, the later methods provide an imprint of the active site geometry without the need for the determination of the protein's structure.

ST6Gal-I is a structurally uncharacterized glycosyltransferase of biomedical importance. It catalyzes the transfer of sialic acid residues from CMP-NeuAc to the terminal galactose residues of glycan chains of glycolipids and glycoproteins on the surfaces of mammalian cells. Variation in the amount of sialic acid incorporated is correlated with colon cancer, brain tumors, and immune regulation in the human body (*9*, *10*). The cDNA encoding ST6Gal-I was first cloned from rat liver (*11*) and biochemically characterized in 1982 (*12*, *13*). However, the structure of ST6Gal-I remains a challenge because of the normal membrane association, native glycosylation, and poor expression in bacterial hosts. Crystal structures of four sialyltransferases of bacterial origin have been reported. They include the 2,3-/2,8-sialyltransferase (CstII) from *Campylobacter jejuni* (OH4384) (*14*), the 2,3-sialyltransferase (Cst-I) from *C. jejuni* (*15*), the 2,3/6-sialyltransferase (Δ24PmST1) from *Pasteurella multocida* strain P-1059 (*16*, *17*), and, most recently, the α-2,6-sialyltransferase (JT-ISH-224) from *Vibrionaceae photobacterium* sp. (*18*). In several cases, these structures have been produced in complex with the inactive donor analogue, CMP-3FNeuAc, or the product, CMP; in the two latter cases, a potential acceptor, lactose, has also been included. Unfortunately, there are no overall sequence similarities between these bacterial sialyltransferases and the mammalian sialyltransferases. The levels of sequence identity for ST6Gal-I and CstII, Cst-I, Δ24PmST1, and JT-ISH-224 are 11, 14, 15,

[†]This work was supported by a grant from the National Center for Research Resources of the National Institutes of Health (RR05351).

*To whom correspondence should be addressed. Phone: (706) 542-6281. Fax: (706) 542-4412. E-mail: jpresteg@ccrc.uga.edu.

[1]Abbreviations: CMP, cytidine 5′-monophosphate; NeuAc, *N*-acetylneuraminic acid; CMP-3FNeuAc, cytidine 5′-monophosphate 3-(axial)-fluoro-*N*-aceytlneuraminic acid; CMP-4carboxyTEMPO, cytidine 5′-monophosphate 4-*O*-(4-carboxy-2,2,6,6-tetramethylpiperidine-1-oxyl); GlcNAc, *N*-acetylglucosamine; Gal, galactose; LacNAc, *N*-acetyllactosamine; LacNAc-TEMPO, *N*-acetyllactosamine 4-*O*-(4-carboxy-2,2,6,6-tetramethylpiperidine-1-oxyl); NMR, nuclear magnetic resonance.

Published on Web 10/21/2009

and 16%, respectively. Currently, no information about the relative orientation of the donor and acceptor co-occupying the active site of ST6Gal-I is available. Also, the differences in reactions conducted by the bacterial sialyltransferases, which include 2−3 and 2−6 donor activities as well as broader acceptor specificities, make it risky to draw conclusions from the position of lactose in the bacterial enzymes about the active site geometries of ST6Gal-I.

There have been a number of examples in which paramagnetic constraints were used to examine distances between substrates and protein residues detected by NMR (*1*, *5*, *19*−*23*). The spin-labeled moiety chosen here is the commonly used and chemically stable TEMPO moiety (2,2,6,6-tetramethylpiperidine-1-oxyl). Its nitroxide group contains an unpaired electron that can significantly increase relaxation rates of protons and other magnetic nuclei. The effect is relatively long-range because the electron magnetic moment is 658 times larger than the proton magnetic moment and even larger when compared to those of most other nuclei. Effects also are easily measured; as the spin relaxation times are shortened (in particular T_2), the protein resonances are broadened and the cross-peak intensity in most multidimensional experiments is reduced. The general procedure is first to acquire a spectrum of the protein with the spin-labeled ligand in its oxidized form, and then again after reduction of the nitroxide radical with ascorbate. The peak intensity differences in the oxidized and reduced spectra should be directly attributable to the paramagnetic relaxation enhancement and simply related to r^{-6}. These effects can be observed up to 20 Å or more in most protein $^{1}H-^{15}N$ HSQC experiments, allowing distances between the nitroxide spin and the nuclei giving rise to the cross-peaks to be calculated.

Similar distance-dependent perturbations can be measured for the ligand in lieu of the protein. The protein sample does not need isotope labeling, and sites in the ligand (usually $^{1}H-^{13}C$) can be detected at natural abundance as long as rapid exchange exists and a sufficiently high concentration of the ligand can be used. In principle, relaxation perturbation of an exchanging ligand in the presence of a second exchanging ligand carrying a nitroxide group can be measured from any type of relaxation parameter. There are certain advantages in measuring longitudinal relaxation times (T_1) rather than the transverse relaxation time (T_2) often measured in protein systems, including the fact that exchanging ligands usually suffer some resonance broadening due to intermediate exchange rates on and off the protein. These exchange broadening effects can be difficult to separate from the paramagnetic T_2 effects. As long as the exchange is fast compared to T_1, T_1 values are not affected by the exchange process. In choosing between T_1 values of protons or carbons, we find T_1 values of carbon have an advantage because T_1 values of protons in large complexes suffer from spin diffusion. There may be some concern about effects of direct electron transfer for heteronuclei which has been postulated when paramagnetic metals are used (*24*). However, to the best of our knowledge, these effects have not been documented for nitroxides.

Transferred nuclear Overhauser (trNOE) and saturation transfer difference (STD) experiments are common methods for determining bound conformations and binding motifs of substrates bound to proteins (*25*). Transferred NOE experiments are able to demonstrate a substrate's binding to a macromolecule and provide distance restraints between proximate pairs of protons in the substrate itself. When ligand molecules bind to large receptor proteins, NOEs undergo drastic changes leading to the observation of strong negative trNOEs as opposed to the normally weak and positive NOEs of small ligands. Because of the dominance of bound ligand properties in the measured NOE, these negative NOEs can be converted to distance restraints for proximate pairs of ligand protons, as they exist in the bound state.

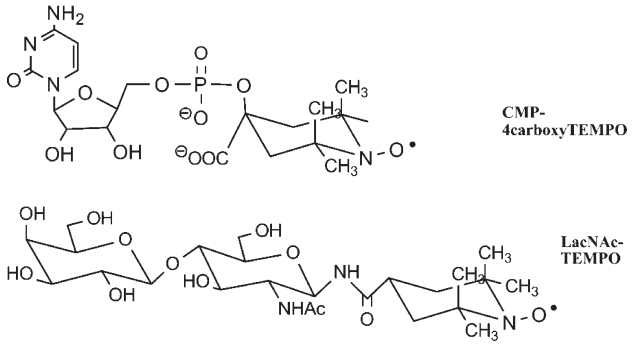

FIGURE 1: Structures of the spin-labeled substrates of ST6Gal-I. CMP-4carboxyTEMPO is a donor mimic, while LacNAc-TEMPO is an acceptor.

In STD experiments, the binding epitope of the substrates can be determined by assessing saturation transfer from protein protons to the individual protons of the substrates when the protein is saturated. In one-dimensional (1D) ^{1}H experiments, a cascade of Gaussian-shaped pulses is applied to the aliphatic protons of protein. The resultant regional saturation quickly diffuses through the protein by intramolecular spin diffusion and then to the ligand protons by intermolecular spin diffusion. Because of the fast exchange of free and bound ligands, the saturation carried by the ligands is transferred into solution and detected as a saturation of specific protons in the solution form of the ligand. By subtracting this spectrum from a spectrum with protein irradiated at a frequency well away from its proton resonances, we obtain a NMR spectrum in which the intensities of ligand signals are reduced in proportion to the proximity of ligand protons to protons on the protein surface.

In what follows, a spin-labeled acceptor, LacNAc-TEMPO (*21*) (Figure 1), has been used to observe changes in additional resonances of [^{15}N]Phe-labeled ST6Gal-I, and these have been compared to previous changes observed during the binding of a spin-labeled donor. The donor analogue, CMP-4carboxyTEMPO (Figure 1), is then used to perturb resonances of a non-spin-labeled acceptor, *N*-acetyllactosamine (LacNAc). Distances between the nitroxide of the donor and the acceptor are estimated on the basis of carbon T_1 changes for the acceptor in the presence and absence of the spin-labeled donor. A ^{13}C-labeled version of LacNAc was incorporated to improve the precision of relaxation rate measurements which were conducted via indirect detection of carbons through protons in arrayed HSQC experiments. Finally, these new data were combined with results from trNOEs and STD experiments to provide insight into how both the donor and acceptor are positioned in the active site of ST6Gal-I.

MATERIALS AND METHODS

The synthesis of LacNAc-TEMPO has been published (*21*); the preparation of [^{15}N]Phe-labeled ST6Gal-I has likewise been reported previously (*5*).

Two-Step Enzymatic Synthesis of CMP-3FNeuAc. *N*-Acetylmannosamine, 3-fluoropyruvate, cytidine triphosphate,

and NeuAc aldolase (EC 4.1.3.3) were purchased from Sigma-Aldrich. CMP-NeuAc synthetase (EC 2.7.7.43) was purchased from Calbiochem. CMP-3FNeuAc was synthesized using CMP-NeuAc synthetase to react cytidine triphosphate with 3-fluoro-NeuAc which was prepared from the reaction of 3-fluoropyruvate and *N*-acetylmannosamine catalyzed by NeuAc aldolase (*26*). The purification of the CMP-3FNeuAc product was conducted by centrifugation, ethanol precipitation (9:1, v/v) (*27*), and size exclusion chromatography on a Biogel P2 column (extra fine, water, 4 °C). The overall yield was 77%.

Three-Step Enzymatic Synthesis of ^{13}C-Enriched LacNAc. $^{13}C_6$-labeled GlcNAc and $^{13}C_6$-labeled Gal were purchased from Omicron Biochemicals, and the remaining reagents were purchased from Sigma-Aldrich. The following enzymes were used, galactokinase (EC 2.7.1.6) purified in the lab following the literature procedure (*28*), galactose-1-phosphate uridyltransferase (EC 2.7.7.12) from Sigma-Aldrich, and galactosyltransferase (EC 2.4.1.90) from Calbiochem. A solution (1.5 mL) containing 50 mM Tris-HCl, 5 mM Mg^{2+}, 20 mM ATP, and 20 mM Gal or [$^{13}C_6$]Gal at pH 7.9 was prepared in a 5 mm NMR tube (*29*). Ten units of galactokinase was added, and the reaction was conducted in this tube heated to 85 °C for 40 min. After the reaction mix had cooled to room temperature, 1 unit of Gal-1-phosphate uridyltransferase was added together with 40 mM UDP-glucose. After incubation for 40 min at 37 °C, 1 unit of galactosyltransferase was added with 5 mM $MnCl_2$ and 10 mM GlcNAc or [$^{13}C_6$]GlcNAc, and the pH was adjusted to 7.5. The reaction mixture was left standing overnight at 37 °C. The crude product was purified sequentially by Centricon filtration of enzymes, anion exchange chromatography on a Dowex 1X-2 column (formate form, 1 cm × 10 cm, water) to remove the phosphates, size exclusion chromatography on a Biogel P2 column (extra fine, 1.5 cm × 45 cm, water) to separate the salts, and finally lyophilization to collect 4.9 mg of white solid (yield, 86%).

Purification of Reduced CMP-4carboxyTEMPO. While in situ reduction of nitroxides with ascorbate normally works well, in some cases it is advantageous to add nitroxide in a prereduced form. To prepare this form, the oxyl radical of CMP-4carboxyTEMPO was therefore reduced to a hydroxyl group by the addition of 3 μL of phenylhydrazine to 2.7 mg of CMP-4carboxyTEMPO in 0.5 mL of methanol. After the mixture had been gently swirled for 20 min, the solvent was evaporated on a rotary evaporator. The following steps were mostly conducted under argon: adding 2−3 mL of ether, vortexing, decanting, repeating twice until the supernatant was clear, adding methanol to dissolve the residue and evaporating the solvent, repeating the ether wash twice, and co-evaporating the residue with methanol to remove the remaining ether. The dried sample weighed 2.1 mg. ^{1}H NMR was taken to verify the reduction and complete removal of phenylhydrazine.

Paramagnetic Perturbation of [^{15}N]Phe-Labeled ST6Gal-I NMR Spectra. NMR samples were prepared in 10% D_2O/90% Bis-Tris buffer (20 mM, containing 200 mM NaCl) at pH 6.5 with a protein concentration of 0.3 mM. The spectra were recorded on a Varian INOVA spectrometer operating at 900 MHz for protons. The spectrometer was equipped with a triple-resonance cryogenic probe having z pulsed gradient coils. Spectra were run with the fast HSQC sequence supplied as part of the Varian BioPak. Data were typically acquired at 25 °C with 11990 Hz as SW, 1800 Hz as SW1, 48 indirect t_1 complex points, 514 direct t_2 complex points, and a recycling rate of 1.5 s. Each spectrum represents a total acquisition time of ~3 h using 64 scans at each t_1 point.

T_1 Relaxation Measurements on the Carbons of [^{13}C]LacNAc. NMR samples were prepared in 10% D_2O/90% Bis-Tris buffer (20 mM, containing 200 mM NaCl) at pH 6.5 with a ST6Gal-I concentration of 0.3 mM. The spectra were acquired on a Varian INOVA spectrometer equipped with a cryogenic z gradient probe operating at 800 MHz (for protons). The spectra were run using the ^{13}C T_1 relaxation mode of the gChsqc sequence in the Varian BioPak. Data were typically acquired at 25 °C with 6828 Hz as SW, 7038 Hz as SW1, 64 indirect F_1 complex points, 819 direct F_2 complex points, and a recycling delay of 1.2 s. The relaxation delays after Z storage were 0.01, 0.08, 0.15, 0.25, 0.4, 0.6, 0.9, and 1.3 s. Each set of arrayed HSQC spectra represents a total acquisition time of ~9 h.

trNOE and STD NMR Data. NMR samples were prepared in deuterated 12 mM phosphate buffer (containing 200 mM NaCl) at pH 6.5. The spectra were recorded with the Varian BioPak pulse sequences on Varian INOVA spectrometers operating at 600 or 800 MHz (^{1}H frequency). The trNOE experiments were performed using zero-quantum-filtered two-dimensional (2D) NOESY at an array of mixing times (50 ms, 100 ms, 200 ms, 500 ms, 1 s, and 2 s) and a recycling rate of 1.2 s. The STD experiments followed the saturation transfer 1D protocol (DPFGSE 1D) without a $T_{1\rho}$ filter or solvent saturation and used a 100 Hz Gaussian saturation pulse train of 450 ms centered at 0.8 ppm in the aliphatic region. The off-frequency spectra were recorded by irradiation at 24 ppm. The recycling delay was 2.5 s.

Calculation of Distances from Relaxation Enhancements. T_1 spin relaxation data were fit to single-exponential curves using Rate Analysis in NMRView. The extracted relaxation rates ($R_1 = T_1^{-1}$) were then related to distances between the spin-label and the site of measurement using the following equations:

$$R_{1C(NO)}/R_{1CH} = [r_{CH}/r_{C(NO)}]^6(\gamma_E/\gamma_H)^2 \quad (\times 0.5 \text{ for the two protons on C6 carbons}) \quad (1)$$

$$R_{1CHobs} = (1 - F_b)R_{1CHfree} + F_b R_{1CH} \quad (2)$$

$$R_{1C(NO)obs} = (1 - F_b')R_{1CHfree} + F_b'[R_{1CH} + R_{1C(NO)}] \quad (3)$$

where R_{1CH} is the relaxation rate due to protons directly bound to carbons, $R_{1C(NO)}$ is the relaxation rate contribution due to the presence of the nitroxide electron, $R_{1CHfree}$ is the relaxation rate contribution from the acceptor free in solution, R_{1CHobs} is the relaxation rate observed in the presence of non-spin-label donor analogues and protein, $R_{1C(NO)obs}$ is the relaxation rate observed in the presence of CMP-4carboxyTEMPO and protein, F_b refers to the fraction of acceptor complexed with non-spin-label donor analogues, and F_b' refers to the fraction of acceptor complexed with CMP-4carboxyTEMPO in the protein solution. The C−H bond length (r_{CH}) used in the calculations was 1.09 Å. The scaling factor (4.25×10^5) in eq 1 is based on an estimated correlation time for the protein of 20 ns and contains dependencies on gyromagnetic ratios of the unpaired electron γ_E (-1.76×10^{11}) and the ^{1}H nuclei γ_H (2.68×10^8).

RESULTS

Paramagnetic Perturbation of [^{15}N]Phe-Labeled ST6Gal-I by Spin-Labeled Acceptor LacNAc-TEMPO. An HSQC spectrum of a 0.3 mM ST6Gal-I sample prepared with

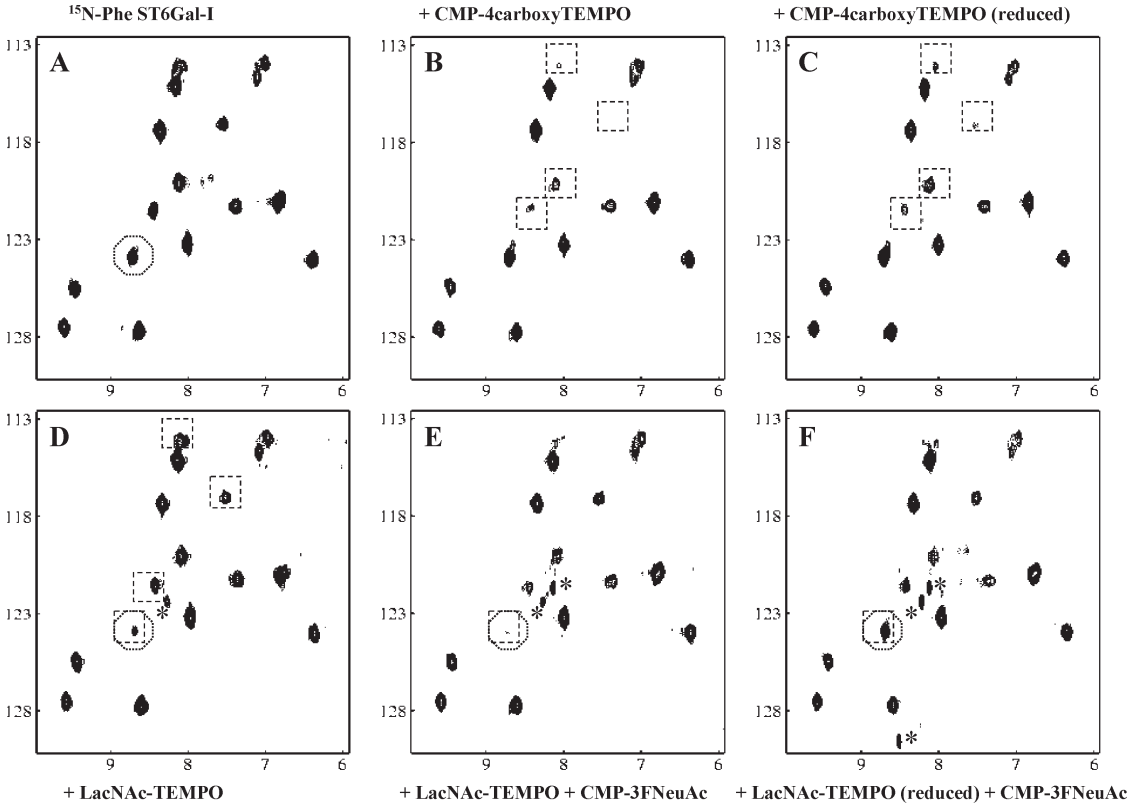

FIGURE 2: ^{1}H−^{15}N HSQC spectra of [^{15}N]Phe-labeled ST6Gal-I in the presence of the indicated substrates. (A) [^{15}N]Phe-labeled ST6Gal-I in the absence of substrates. (B and C) [^{15}N]Phe-labeled ST6Gal-I with a 4-fold molar excess of CMP-4carboxyTEMPO (B) before and (C) after reduction using ascorbate. (D−F) [^{15}N]Phe-labeled ST6Gal-I with a 20-fold excess of LacNAc-TEMPO (D) and an added 15-fold excess of CMP-3FNeuAc (E) and added ascorbate (F). The boxed peaks were broadened due the presence of spin-labeled substrates. The circled peak was most strongly perturbed and was used to estimate structural changes in ST6Gal-I upon addition of CMP-3FNeuAc. The circled peak did not change upon the addition of solely CMP-3FNeuAc to ST6Gal-I (Figure 2B in ref *2*). Additional peaks that appeared because of natural abundance ^{15}N−H in the NH-NeuAc moiety of CMP-3FNeuAc or the GlcNAc moiety of LacNAc-TEMPO are denoted with an asterisk.

all phenylalanines labeled with ^{15}N is presented in Figure 2A. It shows 16 cross-peaks (not yet assigned) corresponding to the 16 labeled amide sites in ST6Gal-I. When a 4-fold excess of CMP-4-carboxyTEMPO was added, four of the 16 protein cross-peaks were perturbed by the presence of a spin-label (*5*) (boxed in Figure 2B). Just as in previous work with the sugar donor analogue, CMP-4carboxyTEMPO, we can identify cross-peaks belonging to phenylalanines near the LacNAc-binding site based on the steep $1/r^6$ distance dependence of the effects.

Before cross-peaks with proximity to the binding site can be correlated, appropriate controls must be run. Since ligand exchange dynamics can lead to peak broadening and intensity loss, it is important to compare spectra with a nonparamagnetic ligand having a structure as close as possible to that of the TEMPO analogue. The simplest way to do this is to reduce the TEMPO analogue. When the nitroxide radical was reduced by sodium ascorbate, the partial or complete reappearance of the perturbed resonances of the protein was observed (Figure 2C). Changes in intensities between reduced and oxidized spectra were then related to distances between the nitroxide and the corresponding phenylalanines. The possibility of nonspecific binding of the TEMPO moiety to secondary sites was also excluded by a control experiment in which ST6Gal-I was titrated with 4-carboxyTEMPO; no changes were observed for protein resonances.

LacNAc-TEMPO perturbs three of the four peaks seen with CMP-4carboxyTEMPO (Figure 2D). This confirms binding of the donor near the acceptor site. However, there are significant differences. For example, one peak almost completely disappears in the presence of LacNAc-TEMPO (circled in Figure 2D) but was not perturbed by CMP-4carboxyTEMPO. Nor was this peak perturbed by the nonparamagnetic donor mimic CMP-3FNeuAc which broadened three other protein peaks (*5*). A change in this particular peak did, however, occur when CMP-3FNeuAc was included along with LacNAc-TEMPO (Figure 2E). Integrations of the peaks show that the intensity of the circled peak decreases an additional factor of 2 upon comparison of Figure 2D to Figure 2E, and the peak reappeared to full intensity when the nitroxide was quenched (Figure 2F). The additional decrease could come from enhanced binding of the LacNAc-TEMPO molecule in the presence of a donor. Cooperative binding of the donor and acceptor has been suggested for a number of glycosyltransferases (*16*, *30*−*32*). The decrease could also come from a conformational change in the glycosyltransferase induced on donor binding. The latter types of conformational change have also been documented in other glycosyltransferases (*16*, *33*). We believe the latter to be the explanation in the current case, because, even in the absence of sugar donor, the binding site was nearly saturated at the concentrations of LacNAc-TEMPO used. On the basis of a fixed fraction of bound LacNAc-TEMPO, it is estimated that the donor brought the acceptor 6% closer to the ^{15}N-labeled Phe associated with the perturbed peak (see eq 1 in ref *5*). This observation is consistent with a loop movement seen in Δ24PmST1 in which a buried tryptophan flips out of the protein core to redefine the acceptor binding site once the donor binds to the protein (*16*).

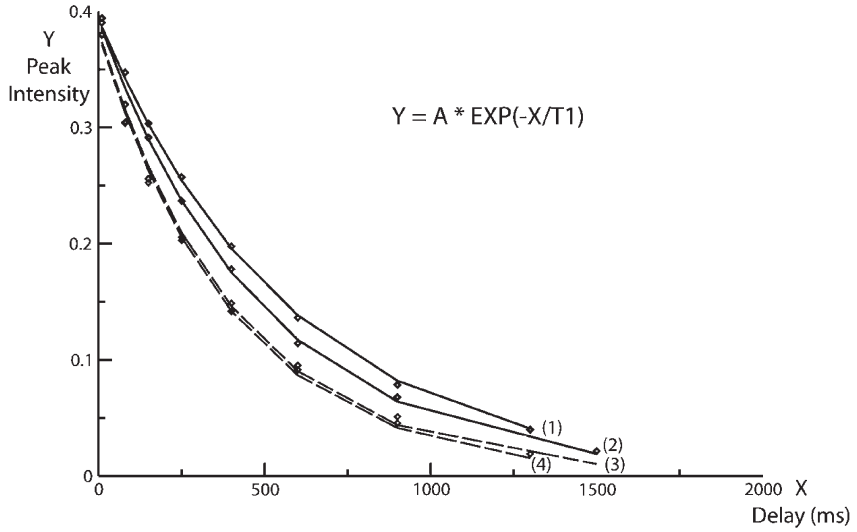

FIGURE 3: T_1 measurement examples for the carbon of Gal4 (solid black line) and the carbon of Gal6 (dashed gray line) with and without spin-label perturbation by CMP-4carboxyTEMPO binding to the protein. (1) Data for Gal4 without a spin-label. The T_1 was calculated to be 574 ms. (2) Data for Gal4 with a spin-label. The T_1 was calculated to be 496 ms. (3) Data for Gal6 with a spin-label. The T_1 was calculated to be 416 ms. (4) Data for Gal6 without a spin-label. The T_1 was calculated to be 406 ms.

Relaxation Enhancement of the Bound Acceptor by a Bound Spin-Labeled Donor Analogue. The relative positions of the bound acceptor and bound donor analogue can also be probed using paramagnetic perturbations. The paramagnetic relaxation enhancement of the bound acceptor due to bound CMP-4carboxyTEMPO was measured by comparing the T_1 values of acceptor carbons in control and in relaxation-enhanced samples. The enhancements were in turn converted into intermolecular distances between the substrates in the protein binding site. The relaxation-enhanced sample contained 0.3 mM ST6Gal-I, 1.0 mM [^{13}C]LacNAc, and a near-saturating amount of CMP-4carboxyTEMPO [3 mM; estimated at 79% saturation of protein using a dissociation constant (K_D) of 0.75 mM (*5*)]. The two control samples contained ST6Gal-I, the acceptor, and the equivalent amount of CMP-3FNeuAc or reduced CMP-4carboxyTEMPO. T_1 values of carbons were calculated from peak intensities measured in an arrayed ^{1}H$-^{13}$C HSQC experiment in which an extra z-storage, relaxation delay, and *J* evolution element had been inserted just before the INEPT transfer back to protons. Examples of the data are given in Figure 3 which depicts exponential fits to a resonance showing a significant change in T_1 (that from C4 of the galactose residue in LacNAc) and a resonance showing minimal perturbation (that from C6 of the galactose residue in LacNAc).

The changes in the longitudinal relaxation rate (R_1, T_1^{-1}) for the sugar residues are actually small, ranging from 0.05 to 0.37 s^{-1} (Figure 4). This is partly due to the fact that paramagnetic effects on heteronuclear longitudinal relaxation rates by nitroxide are inherently small at high magnetic fields and partly due to the small fraction of the acceptor bound to ST6Gal-I while CMP-4carboxyTEMPO also was binding. With an estimated K_D value of 1.6 mM for the acceptor, the experimental sample of 0.3 mM ST6Gal-I, 1.0 mM acceptor, and 3 mM CMP-4carboxyTEMPO would yield only 9% of the acceptor bound to CMP-4carboxyTEMPO-occupied ST6Gal-I. Clearly, it would be advantageous to have acceptor analogues with higher affinities for these experiments. Nevertheless, some useful data can be extracted. The enhanced relaxation rates of C4 of Gal and of C6 of α-GlcNAc are obviously significant. The absolute propagated

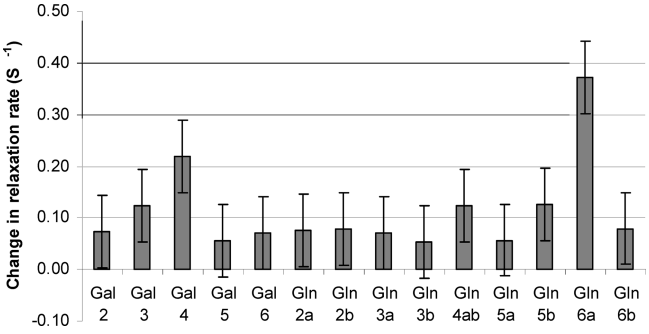

FIGURE 4: Differences in R_1 values of LacNAc carbons in the control and experimental samples. All the changes are positive, and they indicate paramagnetic perturbation from bound CMP-4carboxyTEMPO. The *N*-acetyl methyl carbons were not measured in the ^{1}H$-^{13}$C HSQC spectrum because of the lack of ^{13}C enrichment in the methyl group. The data for Gal1, GlcNAc1α, and GlcNAc1β are not shown because their peak intensities were attenuated by water suppression during the acquisition of spectra.

standard error on average is 0.14 s^{-1} based on the standard error of 5% from the exponential fit of the peak intensity data.

On the basis of the R_1 changes of Gal and GlcNAc carbons between the control and relaxation-enhanced samples (shown in Figure 4), the distances from the donor nitroxide to the 14 acceptor carbons can be calculated. In these calculations, the internal motions of the ligand were ignored and the modulation of interactions by the tumbling correlation time for the protein was assumed to dominate relaxation in all cases. The estimates are dependent on the fraction of acceptor complexed with proteins carrying non-spin-labeled donor analogues, 9.2% for CMP-3FNeuAc and 7.3% for reduced CMP-4carboxyTEMPO, as well as the fraction of acceptor complexed with protein, carrying CMP-4carboxyTEMPO, which is calculated to be 8.9%. The details of the calculation protocol are given in Materials and Methods. The distances calculated range from 8 to 12 Å with 9 Å for Gal4 and 8 Å for GlcNAc6α being the shortest distances. The data are consistent with preferential exposure to nitroxide of carbons on a side of LacNAc where both Gal4 and GlcNAc6 can be exposed.

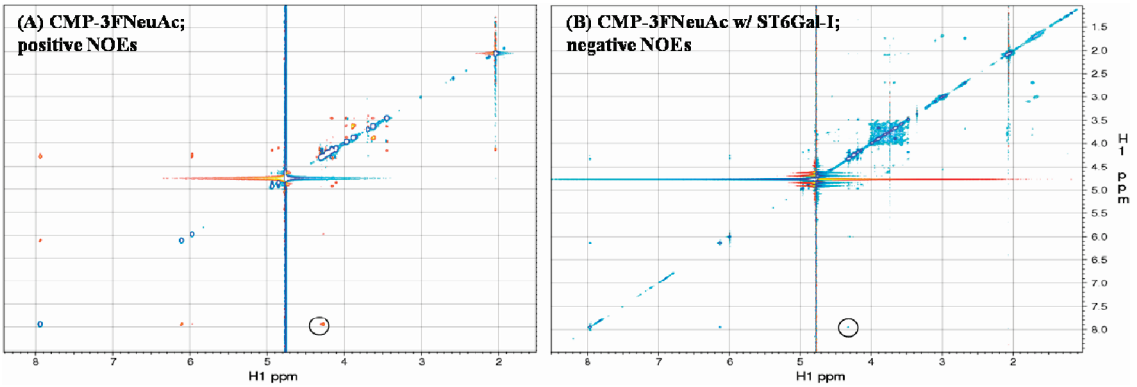

FIGURE 5: $^{1}H-^{1}H$ 2D NOESY spectra of CMP-3FNeuAc (1.5 mM) without (A) and with (B) ST6Gal-I (0.3 mM) at a mixing time of 500 ms and at 25 °C. Red indicates a positive NOE, and blue indicates a negative NOE. No cross-peaks between the cytosine/ribose ring and the NeuAc ring were observed, suggesting long distances. The circled cross-peaks indicate the NOEs connecting cytosine H6 and ribose H3 protons.

Investigation of Bound Conformations from trNOE and Binding Epitopes from STD Experiments. Transferred NOEs can provide useful information about the conformations of the individual bound ligands. Strong negative NOEs were observed from samples having a large excess of CMP-NeuAc and CMP-3FNeuAc in the presence of ST6Gal-I (Figure 5). This clearly indicates the dominance of NOEs by contributions from the ligands in the bound state. In Figure 5, the circled cross-peak connects the H6 proton of the cytosine ring and the H2 and H3 protons of the ribose. This NOE also was strong for CMP-3FNeuAc in the absence of the protein, but it had the opposite sign. This observation in both free and bound states supports the dominant population of the anti conformation about the cytosine−ribose glycosidic bond in which the H6 and H2/H3 protons are in the proximity of each other. Given that the distance from cytosine H5 to cytosine H6 is 2.5 Å, the distance between cytosine H6 and ribose H3 was calculated to be 2.3 Å in the protein-free solution and 2.6 Å in the presence of the protein, based on their respective cross-peak intensities. These values are very close to one another and also close to distances expected on the basis of both predictions of minimum energy structures and the conformations observed in other crystal structures. Unfortunately, there were no cross-peaks detected between the nucleotide and the donor sugar. However, the absence of cross-peaks is consistent with the long distances between nucleotide and sugar protons seen in the preferred low-energy states and the states typically seen in the crystal structures. In modeling structures, we will use these previously observed minimum energy conformers for the bound donor.

Transferred NOE data on the LacNAc acceptor were difficult to collect because of its weak binding to ST6Gal-I. NOEs collected at 25 °C were in fact positive and difficult to distinguish from NOEs seen for LacNAc in the absence of the protein. The dominant NOEs obtained in a 1D NOE experiment, in which the anomeric proton resonance of galactose was saturated, showed the expected intraring connectivity to the axial H3 and H5 protons as well as a poorly resolved but distinguishable connection to the trans-glycosidic GlcNAc H4 proton. The latter observation is consistent with LacNAc favoring the low-energy $\psi = -123.26°$ (C1−O4−C4′−C5′), $\phi = -64.33°$ (O5−C1−O4−C4′) conformation in solution. To make effects of protein binding observable, the temperature was lowered to 17 °C where LacNAc in free solution showed minimal NOEs (actually a mix of positive and negative NOEs, possibly due to a mix of contributions from overall anisotropic motions and internal motions). As depicted in Figure 6, the addition of ST6Gal-I now produces some clear negative NOEs (to Gal H3) and some negative contributions that cancel residual positive contributions at Gal H5 and GlcNAc H4 protons. The GlcNAc H4 contribution is consistent with the maintenance of a dominant population for the minimum energy structure in the bound complex as well.

Saturation transfer difference (STD) experiments were used in an attempt to identify the binding epitopes of both the donor and the acceptor. Saturation transfer is most efficient when protein protons (connected by spin diffusion to a general protein proton pool) are in the proximity of ligand protons. When the saturated spectrum is subtracted from a reference spectrum and protein peaks are removed by subtraction of an STD pair without ligand, the amplitudes of the remaining peaks of the resulting difference spectrum correlate with the proximity of the respective ligand protons to protons on the protein surface. STD data for both CMP-3FNeuAc and the natural donor, CMP-NeuAc, were collected. These data are presented in Figures S1 and S2 of the Supporting Information. Collection of data for the natural donor was of higher quality, but its interpretation was complicated by the slow hydrolysis of the donor because the cytosine H5 and ribose proton resonances from the CMP product overlap resonances from the donor. Data for the nonhydrolyzable CMP-3FNeuAc are summarized in Figure 7. STD percentages of the ligands were calculated as the ratio of individual peak intensities in the corresponding difference spectrum and in the reference spectrum and normalized using the STD effect of the ribose H1 proton. The derived STD percentages of CMP-3FNeuAc show a clear preferential enhancement of the nucleotide base and adjacent parts of the ribose ring over the 3FNeuAc ring. This observation is consistent with the evidence that CMP, contained in both ligands, is an efficient competitive inhibitor of ST6Gal-I. The less efficient magnetization transfer to the sugar residue is consistent with the necessity of having space near the sugar residue to accommodate the acceptor. The binding epitope of CMP-3FNeuAc demonstrates that CMP serves as a recognition motif for ST6Gal-I that provides reasonable affinity for a number of different CMP-sugar donors (*34*).

An STD effect for LacNAc could be detected only when the ratio of the ligand to the protein was ≥35-fold and the sample was cooled to 5 °C. However, the effects were small and quite uniformly distributed over all protons of the LacNAc moiety. This can be the result of binding in a mode where magnetization transfers from protein protons to ligand protons are inefficient compared to intraligand transfers, such as would occur when

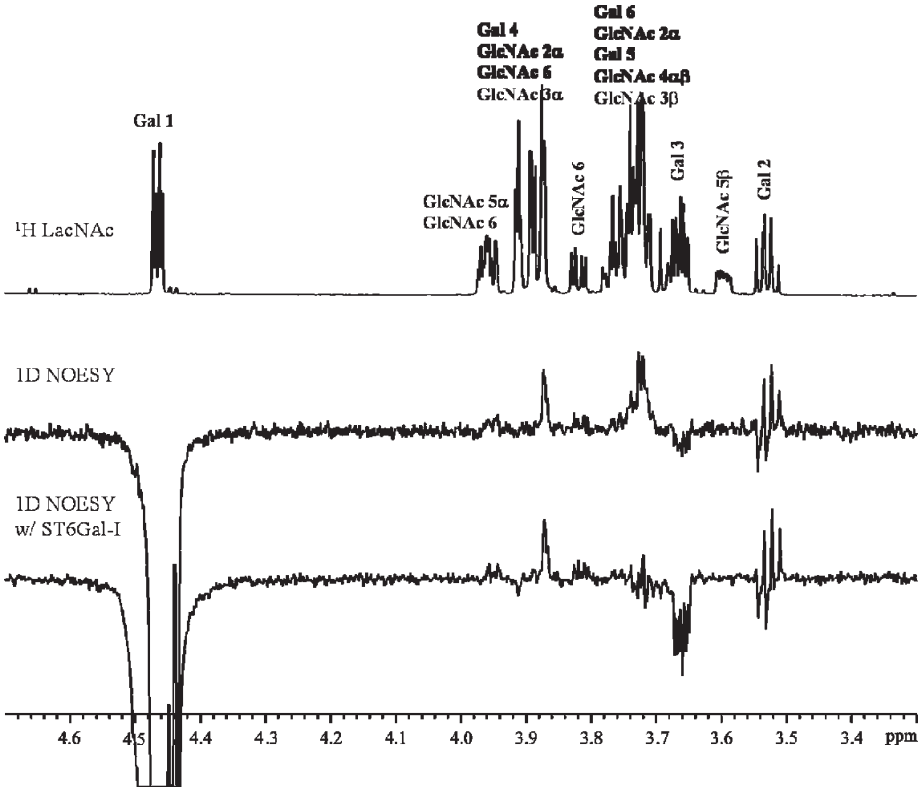

FIGURE 6: ^{1}H NMR spectra of LacNAc and 1D NOESY spectra of LacNAc (4.5 mM) without and with ST6Gal-I (0.3 mM) recorded at 17 °C.

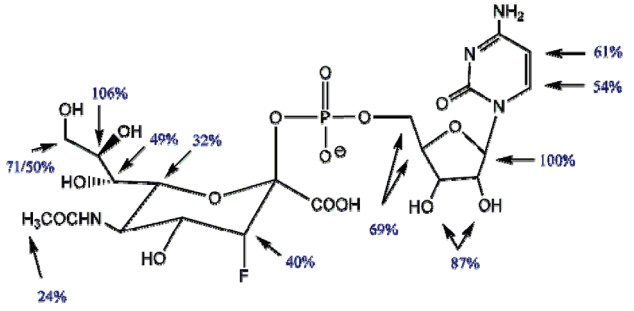

FIGURE 7: Derived STD percentages for the protons of CMP-3FNeuAc (1.5 mM) bound to ST6Gal-I (0.3 mM) at 25 °C. The double-headed arrows denote average STD effects for the protons that are unresolved in the STD difference spectrum.

hydrogen bonding interactions dominate rather than close hydrophobic contacts.

DISCUSSION

On the basis of the data presented here, we can make several statements about the placement of the donor and acceptor in the binding site of ST6Gal-I. Even in the absence of a structure for the protein, this placement can provide insight into a mechanism of action and donor and acceptor modifications that might alter this action. First, we can make some qualitative statements about binding site occupancy and relative placement of the donor and acceptor from the data on perturbation of phenylalanine ^{1}H−^{15}N HSQC cross-peaks using a spin-labeled acceptor analogue. The fact that the acceptor analogue perturbed three of the four peaks that were previously perturbed by a spin-labeled donor analogue suggests that they clearly bind in the same general region on the protein surface. However, the fact that one HSQC cross-peak, not perturbed by the spin-labeled donor analogue, was perturbed by the spin-labeled acceptor analogue suggests that the reducing end of LacNAc (where the spin-label is bound) is well removed from contact with the donor sugar (TEMPO in the donor analogue). This is as it should be in a complex poised for addition of the donor sugar to the nonreducing end of the acceptor. These observations will become more useful as the cross-peaks in the HSQC spectra of ST6Gal-I are assigned and a structure is determined.

In principle, related paramagnetic relaxation enhancement (PRE) experiments using the spin-labeled donor analogue and observed perturbations of HSQC peaks from an acceptor allow determination of approximate distances between carbons of the acceptor and the nitroxide of the donor, and construction of a more complete model for placement of the donor and acceptor in the ST6Gal-I binding site. Perturbations are, however, weak and broadly distributed except for those of two well-separated carbons, Gal4 and GlcNAc6. This may suggest that a distribution of sites is occupied in which the spin-label can make close approaches to either site. This would require, at a minimum, exposure of surfaces on the acceptor carrying these two sites.

Figure 8 depicts a model in which the Gal4 and GlcNAc6 sites are exposed. The structure of α-LacNAc shown here is the minimal energy conformer generated by Glycam Biomolecular Builder (*35*) (also http://glycam.ccrc.uga.edu/). The color code indicates the proximity of the LacNAc carbons to the nitroxide of CMP-4carboxyTEMPO with red for closest (Gal4 and GlcNAc6), yellow for second closest (Gal3, GlcNAc4, and GlcNAc5), and green for the farthest (Gal5, Gal6, GlcNAc2, and GlcNAc3). If we assume the less perturbed side on the acceptor is protected by binding to the protein and represents regions that must be conserved for acceptor recognition, the model is consistent with the pattern of the groups rejecting or accepting modifications in the specificity studies of ST6Gal-I (*36*).

It would be most useful at this point to add the donor to this picture using experimental distances from the nitroxide to Gal C4

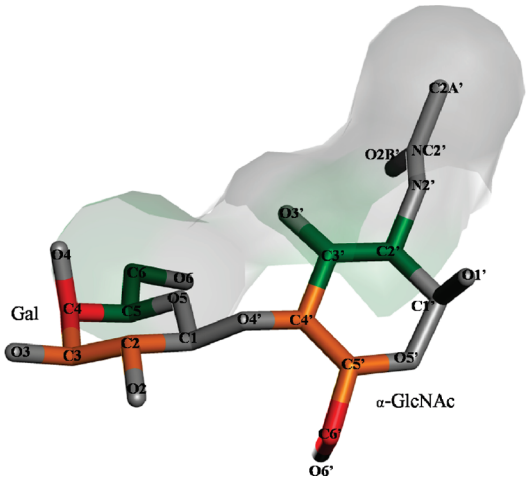

FIGURE 8: Position of α-LacNAc in the active site of ST6Gal-I. The color code indicates the measured proximity from the α-LacNAc carbons to the nitroxide of CMP-4carboxyTEMPO: red for closest (Gal4 and GlcNAc6), yellow for second closest (Gal3, GlcNAc4, and GlcNAc5), and green for farthest (Gal5, Gal6, GlcNAc2, and GlcNAc3). The shaded area is proposed to be protected by the protein surface.

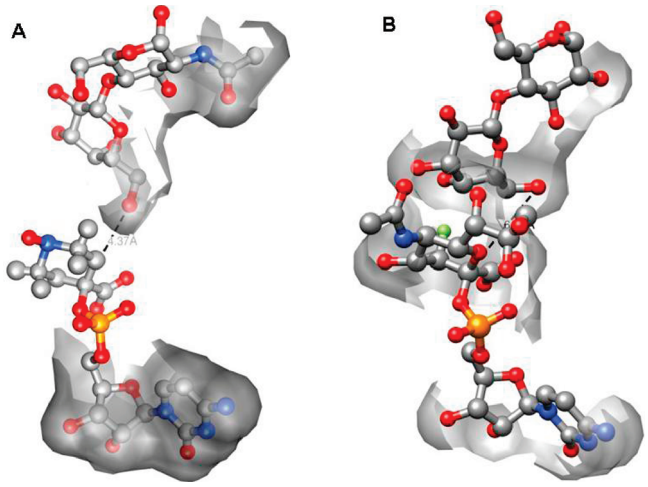

FIGURE 9: Comparison of relative positions and protein surface contacts of the donor and acceptor. (A) CMP-4carboxyTEMPO and α-LacNAc in the ST6Gal-I binding site. (B) CMP-3FNeuAc and α-lactose in the crystal structure of the 2,3/6-sialyltransferase from Δ24PmST1. The dashed lines depict attack on the anomeric carbons of the donor by the O6 atom of the acceptor. The gray regions depict protein contact regions, identified by STD or nitroxide exposure in ST6Gal-I and by the 3.2 Å distance to protein atoms in Δ24PmST1.

and the nitroxide to GlcNAc C6 along with an assumed distance for an SN2 attack of the Gal O6 atom on the C2 atom of the NeuAc residue (~4 Å). Unfortunately, it is not possible to generate models satisfying all three of these closest approach constraints without bringing some other carbons closer. This likely indicates enhanced contributions at C4 and/or C6 due to occupation of secondary binding sites. However, we have produced a best fit model as depicted in Figure 9A. The Gal O6−TEMPO C1 distance is 4.3 Å. The Gal C4−TEMPO N4 distance is 7.5 Å; the GlcNAc C6−TEMPO N4 distance is 8.0 Å, and all other carbons in the LacNAc acceptor are farther from TEMPO N4. The regions depicted in gray represent protein contact regions as determined from STD experiments or protection from contact with the exchanging spin-label.

Comparison to the placement of the donor relative to the acceptor as shown in the crystal structure of bacterial sialyltransferases is of some interest. There are actually two structures of a bacterial 2,3/6-sialyltransferase, Δ24PmST1 from *P. multocida*, reported in the literature and deposited in the Protein Data Bank that have both the donor and acceptor present. Both structures, 2IHZ and 2IY8, have the inactive donor CMP-3FNeuAc bound, but 2IHZ has α-lactose and the 2IY8 *β*-lactose. It has been suggested that the binding orientation of α-lactose in 2IHZ might represent the bound conformation for α-2,6 activity (*16*). The donor−acceptor pair from the crystal structure of 2IHZ is shown in Figure 9B. In this structure, rotating the torsion angle around the C5−C6 bond of Gal can move O6 of Gal from 6.6 Å to within 5.1 Å of the anomeric C2 atom of the donor. Comparison of panels A and B of Figure 9 suggests that the two donor−acceptor pairs occupy similar spatial regions. Both show protein contacts with the nucleotide base and C2−C3 region of the ribose ring. Both show protein contacts with the C2−C3 regions of the Glc or GlcNAc residues of the respective acceptors, and both show protein contacts with the C6 region of the Gal residues of the acceptors. In the crystal structure, there are more contacts with parts of the NeuAc residue of the donor that are not shown on the TEMPO adduct depicted in the figure, but there was a fairly high level of STD transfer (47%) to the H3 proton of the NeuAc residue in experiments conducted with CMP-3FNeuAc and ST6Gal-I. This level of agreement is reasonable given the differences in the enzyme sequences and donor−acceptor pairs used.

While the structure presented cannot yet be considered of sufficient resolution for detailed mechanistic modeling, it does provide a stepping stone for future work. In particular, the sequential assignments of [^{15}N]Phe-labeled ST6Gal-I resonances in the HSQC spectra should add key distances between specific amino acids and the sugar donor to the model. NMR assignment for resonances from proteins that must be expressed in eukaryotic hosts is not a trivial task; however, appropriate methodology is being developed (*37*). Working with higher-affinity acceptors should improve the sensitivity of paramagnetic probes, and orientation-sensitive data such as ligand RDCs (*38*−*40*) should greatly refine the orientation of ligands in the models. With such improvements, we can expect a better structural understanding of ST6Gal-I and a basis for structure-based design of specific inhibitors. The strategies we developed should also find important applications in probing the structures of other glycosyltransferases.

ACKNOWLEDGMENT

We thank Dr. Hans Lee for preparing galactokinase and Dr. Andre Venot for synthesizing LacNAc-TEMPO. We also thank Dr. Megan Macnaughtan, Dr. John Glushka, and Dr. Fang Tian for useful discussion and laboratory assistance.

SUPPORTING INFORMATION AVAILABLE

Data on STD experiments using the ligands CMP-NeuAc and CMP-3FNeuAc. This material is available free of charge via the Internet at http://pubs.acs.org.

REFERENCES

1. Macnaughtan, M. A., Kamar, M., Alvarez-Manilla, G., Venot, A., Glushka, J., Pierce, J. M., and Prestegard, J. H. (2007) NMR structural characterization of substrates bound to N-acetylglucosaminyltransferase V. *J. Mol. Biol. 366*, 1266–1281.

2. Becker, B. A., and Larive, C. K. (2008) Probing the Binding of Propranolol Enantiomers to α_1-Acid Glycoprotein with Ligand-Detected NMR Experiments. *J. Phys. Chem. B 112*, 13581–13587.
3. Constantine, K. L., Davis, M. E., Metzler, W. J., Mueller, L., and Claus, B. L. (2006) Protein-ligand NOE matching: A high-throughput method for binding pose evaluation that does not require protein NMR resonance assignments. *J. Am. Chem. Soc. 128*, 7252–7263.
4. Skinner, A. L., and Laurence, J. S. (2008) High-Field Solution NMR Spectroscopy as a Tool for Assessing Protein Interactions with Small Molecule Ligands. *J. Pharm. Sci. 97*, 4670–4695.
5. Liu, S., Venot, A., Meng, L., Tian, F., Moremen, K. W., Boons, G. J., and Prestegard, J. H. (2007) Spin-labeled analogs of CMP-NeuAc as NMR probes of the α-2,6-sialyltransferase ST6Gal I. *Chem. Biol. 14*, 409–418.
6. Angulo, J., Langpap, B., Blume, A., Biet, T., Meyer, B., Krishna, N. R., Peters, H., Palcic, M. M., and Peters, T. (2006) Blood group B galactosyltransferase: Insights into substrate binding from NMR experiments. *J. Am. Chem. Soc. 128*, 13529–13538.
7. Post, C. B. (2003) Exchange-transferred NOE spectroscopy and bound ligand structure determination. *Curr. Opin. Struct. Biol. 13*, 581–588.
8. Mayer, M., and Meyer, B. (1999) Characterization of ligand binding by saturation transfer difference NMR spectroscopy. *Angew. Chem., Int. Ed. 38*, 1784–1788.
9. Dall′Olio, F., and Chiricolo, M. (2001) Sialyltransferases in cancer. *Glycoconjugate J. 18*, 841–850.
10. Crocker, P. R., Paulson, J. C., and Varki, A. (2007) Siglecs and their roles in the immune system. *Nat. Rev. Immunol. 7*, 255–266.
11. Weinstein, J., Lee, E. U., Mcentee, K., Lai, P. H., and Paulson, J. C. (1987) Primary Structure of β-Galactoside α-2,6-Sialyltransferase: Conversion of Membrane-Bound Enzyme to Soluble Forms by Cleavage of the NH_2-Terminal Signal Anchor. *J. Biol. Chem. 262*, 17735–17743.
12. Weinstein, J., Desouzaesilva, U., and Paulson, J. C. (1982) Purification of a Gal-β-1-]4glcnac α-2-]6 Sialyltransferase and a Gal-β-1-]3(4)Glcnac α-2-]3 Sialyltransferase to Homogeneity from Rat Liver. *J. Biol. Chem. 257*, 3835–3844.
13. Weinstein, J., Desouzaesilva, U., and Paulson, J. C. (1982) Sialylation of Glycoprotein Oligosaccharides N-Linked to Asparagine: Enzymatic Characterization of a Gal-β-1-]3(4)Glcnac α-2-]3 Sialyltransferase and a Gal-β-1-]4glcnac α-2-]6 Sialyltransferase from Rat Liver. *J. Biol. Chem. 257*, 3845–3853.
14. Chiu, C. P. C., Watts, A. G., Lairson, L. L., Gilbert, M., Lim, D., Wakarchuk, W. W., Withers, S. G., and Strynadka, N. C. J. (2004) Structural analysis of the sialyltransferase CstII from *Campylobacter jejuni* in complex with a substrate analog. *Nat. Struct. Mol. Biol. 11*, 163–170.
15. Chiu, C. P. C., Lairson, L. L., Gilbert, M., Wakarchuk, W. W., Withers, S. G., and Strynadka, N. C. J. (2007) Structural analysis of the α-2,3-sialyltransferase cst-i from *Campylobacter jejuni* in apo and substrate-analogue bound forms. *Biochemistry 46*, 7196–7204.
16. Ni, L. S., Chokhawala, H. A., Cao, H. Z., Henning, R., Ng, L., Huang, S. S., Yu, H., Chen, X., and Fisher, A. J. (2007) Crystal structures of *Pasteurella multocida* sialyltransferase complexes with acceptor and donor analogues reveal substrate binding sites and catalytic mechanism. *Biochemistry 46*, 6288–6298.
17. Ni, L. S., Sung, M. C., Yu, H., Chokhawala, H., Chen, X., and Fisher, A. J. (2006) Cytidine 5′-monophosphate (CMP)-induced structural changes in a multifunctional sialyltransferase from *Pasteurella multocida*. *Biochemistry 45*, 2139–2148.
18. Kakuta, Y., Okino, N., Kajiwara, H., Ichikawa, M., Takakura, Y., Ito, M., and Yamamoto, T. (2008) Crystal structure of *Vibrionaceae photobacterium* sp JT-ISH-224 α-2,6-sialyltransferase in a ternary complex with donor product CMP and acceptor substrate lactose: Catalytic mechanism and substrate recognition. *Glycobiology 18*, 66–73.
19. Battiste, J. L., and Wagner, G. (2000) Utilization of site-directed spin labeling and high-resolution heteronuclear nuclear magnetic resonance for global fold determination of large proteins with limited nuclear Overhauser effect data. *Biochemistry 39*, 5355–5365.
20. Ramos, A., and Varani, G. (1998) A new method to detect long-range protein-RNA contacts: NMR detection of electron-proton relaxation induced by nitroxide spin-labeled RNA. *J. Am. Chem. Soc. 120*, 10992–10993.
21. Jain, N. U., Venot, A., Umemoto, K., Leffler, H., and Prestegard, J. H. (2001) Distance mapping of protein-binding sites using spin-labeled oligosaccharide ligands. *Protein Sci. 10*, 2393–2400.
22. Johnson, P. E., Brun, E., MacKenzie, L. F., Withers, S. G., and McIntosh, L. P. (1999) The cellulose-binding domains from *Cellulomonas fimi* β-1,4-glucanase CenC bind nitroxide spin-labeled cellooligosaccharides in multiple orientations. *J. Mol. Biol. 287*, 609–625.
23. Kuliopulos, A., Westbrook, E. M., Talalay, P., and Mildvan, A. S. (1987) Positioning of a Spin-Labeled Substrate-Analog into the Structure of Δ-5−3-Ketosteroid Isomerase by Combined Kinetic, Magnetic-Resonance, and X-Ray-Diffraction Methods. *Biochemistry 26*, 3927–3937.
24. Hansen, D. F., and Led, J. J. (2004) Mapping the electronic structure of the blue copper site in plastocyanin by NMR relaxation. *J. Am. Chem. Soc. 126*, 1247–1252.
25. Meyer, B., and Peters, T. (2003) NMR spectroscopy techniques for screening and identifying ligand binding to protein receptors. *Angew. Chem., Int. Ed. 42*, 864–890.
26. Watts, A. G., and Withers, S. G. (2004) The synthesis of some mechanistic probes for sialic acid processing enzymes and the labeling of a sialidase from *Trypanosoma rangeli*. *Can. J. Chem. 82*, 1581–1588.
27. Knorst, M., and Fessner, W. D. (2001) CMP-sialate synthetase from *Neisseria meningitidis*: Overexpression and application to the synthesis of oligosaccharides containing modified sialic acids. *Adv. Synth. Catal. 343*, 698–710.
28. Verhees, C. H., Koot, D. G. M., Ettema, T. J. G., Dijkema, C., De Vos, W. M., and Van Der Oost, J. (2002) Biochemical adaptations of two sugar kinases from the hyperthermophilic archaeon *Pyrococcus furiosus*. *Biochem. J. 366*, 121–127.
29. Gilhespymuskett, A. M., Partridge, J., Jefferis, R., and Homans, S. W. (1994) A Novel C-13 Isotopic Labeling Strategy for Probing the Structure and Dynamics of Glycan Chains in-Situ on Glycoproteins. *Glycobiology 4*, 485–489.
30. Boix, E., Zhang, Y. N., Swaminathan, G. J., Brew, K., and Acharya, K. R. (2002) Structural basis of ordered binding of donor and acceptor substrates to the retaining glycosyltransferase, α-1,3-galactosyltransferase. *J. Biol. Chem. 277*, 28310–28318.
31. Ramakrishnan, B., Boeggeman, E., Ramasamy, V., and Qasba, P. K. (2004) Structure and catalytic cycle of β-1,4-galactosyltransferase. *Curr. Opin. Struct. Biol. 14*, 593–600.
32. Unligil, U. M., and Rini, J. M. (2000) Glycosyltransferase structure and mechanism. *Curr. Opin. Struct. Biol. 10*, 510–517.
33. Qasba, P. K., Ramakrishnan, B., and Boeggeman, E. (2005) Substrate-induced conformational changes in glycosyltransferases. *Trends Biochem. Sci. 30*, 53–62.
34. Blixt, O., Han, S. F., Liao, L., Zeng, Y., Hoffmann, J., Futakawa, S., and Paulson, J. C. (2008) Sialoside analogue arrays for rapid identification of high affinity siglec ligands. *J. Am. Chem. Soc. 130*, 6680–6681.
35. Kirschner, K. N., Yongye, A. B., Tschampel, S. M., Gonzalez-Outeirino, J., Daniels, C. R., Foley, B. L., and Woods, R. J. (2008) GLYCAM06: A generalizable Biomolecular force field. Carbohydrates. *J. Comput. Chem. 29*, 622–655.
36. Wlasichuk, K. B., Kashem, M. A., Nikrad, P. V., Bird, P., Jiang, C., and Venot, A. P. (1993) Determination of the Specificities of Rat-Liver Gal(β-1−4)Glcnac α-2,6-Sialyltransferase and Gal(β-1−3/4)Glcnac α-2,3-Sialyltransferase Using Synthetic Modified Acceptors. *J. Biol. Chem. 268*, 13971–13977.
37. Nkari, W. K., and Prestegard, J. H. (2009) NMR Resonance Assignments of Sparsely Labeled Proteins: Amide Proton Exchange Correlations in Native and Denatured States. *J. Am. Chem. Soc. 131*, 5344–5349.
38. Seidel, R. D., Zhuang, T. D., and Prestegard, J. H. (2007) Bound-state residual dipolar couplings for rapidly exchanging ligands of His-tagged proteins. *J. Am. Chem. Soc. 129*, 4834–4839.
39. Zhuang, T. D., Leffler, H., and Prestegard, J. H. (2006) Enhancement of bound-state residual dipolar couplings: Conformational analysis of lactose bound to galectin-3. *Protein Sci. 15*, 1780–1790.
40. Zhuang, T. D., Lee, H. S., Imperiali, B., and Prestegard, J. H. (2008) Structure determination of a galectin-3-carbohydrate complex using paramagnetism-based NMR constraints. *Protein Sci. 17*, 1220–1231.